Solid-State Electronics 230 (2025) 109257

Contents lists available at ScienceDirect

Solid State Electronics

journal homepage: www.elsevier.com/locate/sse

Monte Carlo analysis of hot electron injection in the passivation layer of GaN HEMTs☆,☆☆

Pierpaolo Palestri [a,*], Luca Sayadi [b], Andrea Minetto [c], Gerhard Prechtl [b], Luca Selmi [a], Oliver Häberlen [b]

[a] DIEF, University of Modena and Reggio Emilia, Via Vivarelli 10, Modena, 41125, Italy
[b] Infineon Technologies Austria AG, Villach, Austria
[c] Infineon Technologies Americas Corp., El Segundo, CA, USA

ARTICLE INFO

Keywords:
Monte Carlo
Gallium-Nitride
High electron mobility transistor (HEMT)

ABSTRACT

We investigate the injection of hot electrons in the passivation layer above the drift region of GaN HEMTs by means of Monte-Carlo transport simulations. We find that the lateral component of the electric field in the AlGaN layer delivers a non-negligible kinetic energy to the electrons, thus enhancing injection in the passivation at the top, an effect that is not captured by the standard hot-carrier injection models developed for Si devices that requires the development of ad-hoc hot-carrier injection models for GaN devices. The implications of our calculations for the understanding of reliability and dynamic-R_{on} are also briefly discussed.

1. Introduction

Gallium-Nitride (GaN) HEMTs are strong contenders in the area of power electronics, thanks to the large breakdown field and high mobility [1,2] offered to device designers. They exploit the polarization charge at the interface between the GaN and AlGaN layers to create a large electron sheet charge density and achieve a low on-resistance (R_{on}). However, electron trapping in the carbon-doped GaN buffer, and in the passivation layer above the AlGaN, induces detrimental dynamic-R_{on} effects [3–6]. While the former effect has been analyzed in detail [7–10], this work focuses on the much less studied injection of hot electrons in the passivation layer at the top of the AlGaN. This effect may become especially critical in hard-switching applications when the HEMT experiences simultaneously a large drain–source voltage and a large drain current.

Since the vertical component of the electric field in the AlGaN layer repels electrons toward the two-dimensional electron gas (2DEG), only hot electrons can diffuse uphill and get trapped in the passivation layer, possibly causing drifts and device instabilities [11,12]. Therefore, far-from-equilibrium transport simulations (e.g., by the Monte Carlo method) are mandatory to accurately predict the flux of carriers impinging on the passivation/AlGaN interface, which is not captured by standard drift–diffusion models used for this kind of investigation [3, 13,14]. Monte Carlo simulations of electron transport in GaN have been presented in the literature, e.g. in [15–19]. However, they mostly focus on band structures, scattering rate calculations and simulation of uniform transport in bulk GaN.

In this work, we employ an in-house Monte Carlo simulator with analytical bands to solve the Boltzmann transport equation in a template vertical slice representative of the drift region of a GaN HEMT and compute the flux of electrons injected into the passivation to assess how it depends on the vertical and lateral electric field and on the various energy barriers. The simulator is described in Section 2. Results are reported in Section 3. Conclusive remarks and future perspectives are given in Section 4.

2. The Monte Carlo simulator

The left panel in Fig. 1 sketches the cross section of a GaN HEMT. To gain physical insights on the functional dependence of the hot-electron flux into the passivation (Φ) on the vertical and lateral electric field components, we restrict our analysis to a single template slice in the drift region. This is reasonable since the electric field in the drift region varies slowly along x compared to the mean free path, which is in the nm range for hot-electrons, so that the electron distribution function, $f(E)$, depends uniquely on the local electric field, $\vec{F}$. In the simulated slice, we set a given constant lateral field, F_x, and assume a vertical component of the electric field, F_z, with constant but different values in

☆ This article is part of a Special issue entitled: 'EuroSOI-ULIS 2025' published in Solid State Electronics.
☆☆ The review of this paper was arranged by Francisco F. Gamiz.
* Corresponding author.
E-mail address: pierpaolo.palestri@unimore.it (P. Palestri).

https://doi.org/10.1016/j.sse.2025.109257

Available online 10 October 2025

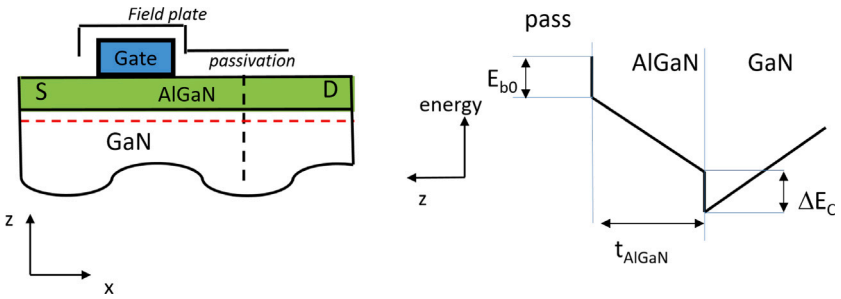

Fig. 1. (left) Sketch of a GaN/AlGaN HEMT, and (right) conduction band diagram along the vertical dashed line in the drift region. The red horizontal dashed line denotes the 2DEG. We consider only the upmost top layers, e.g. the undoped GaN and AlGaN layers. The substrate (Si, SiC, other) and the different buffer layers connecting it with the top GaN are not included in the model, so that results are not specific to a substrate material.

GaN and AlGaN, due to the polarization charge at the interface. These fields are taken as parameters and varied in a realistic range consistent with TCAD simulations of realistic devices featuring field-plates. The result are thus general, and apply to power devices of different voltage classes, bias conditions and design.

Notice that the field component $F_{z,\mathrm{GaN}}$ (see the right panel of Fig. 1) pushes the electrons toward the GaN/AlGaN interface. Some electrons can overcome the conduction band discontinuity ΔE_C and enter the AlGaN, where the repulsive $F_{z,\mathrm{AlGaN}}$ pushes them back toward the GaN. A fraction of these electrons can reach the AlGaN/passivation boundary, where trapping into interface states, and/or thermionic emission above the E_{b0} barrier and subsequent trapping into bulk states, can lead to charge accumulation and drift of the device characteristics. The value of E_{b0} is taken as a free parameter without a direct link to specific passivation materials and processes, that can result in a wide range of possible barriers for electron injection.

Although full-band simulators for GaN have been presented by many authors (e.g. [19–21]), the dominant Γ_1 valley retains a non-parabolic energy dispersion up to high energies close to 2 eV, where satellite valleys come into play. Scattering rates from full-band calculations do not significantly differ from the ones using analytical bands, see [19]. This supports our choice to adopt analytical non-parabolic spherical bands for the Γ_1, Γ_3, and U valleys. The U-Γ_1 band offset is set to 2 eV. Polar and non-polar, acoustic and optical phonon scattering, and alloy scattering in the $Al_{0.2}Ga_{0.8}N$ layer are included in the calculation.

Piezo-electric and Coulomb scattering are implemented too. They significantly impact the mobility, which goes from 1900 $cm^2/(Vs)$ when only phonons are included, to 1500 $cm^2/(Vs)$ and 800 $cm^2/(Vs)$ for doping levels of 10^{15} cm^{-3} and 10^{17} cm^{-3}, respectively, consistently with the MC results in [17] and literature data therein. On the other hand, they play a modest role in the analysis of hot-electrons: we have verified that the flux of injected electrons changes by less than 1% when these mechanisms are included, which is in the order of the statistical error of the MC procedure.

The band and scattering rate parameters (Table 1) are taken from various works on Monte Carlo simulations of bulk GaN and GaN-based devices [15–19].

In addition to the assumptions listed above (single slice with fixed and constant electric fields and E_{b0} taken as parameters), two other main assumptions are discussed below. Electron quantization in the 2DEG is not included. We are indeed analyzing conditions where the lateral electric field is large and heats the electrons, so that most of them are outside the quantum well at the GaN/AlGaN interface. The simulator thus considers a single electron free to move in the real space. For the same reason, we do not enforce Pauli's exclusion principle (that would imply checking the availability of an empty state-after-scattering), since the electron population is spread over a large energy range, keeping the state occupation well below 1. Not enforcing Pauli's exclusion principle makes the quantities provided by the MC algorithm to scale linearly with the electron sheet density N_{2D}.

Table 1
GaN model parameters of the Monte Carlo transport simulator. The energy offsets $\Delta E_{\Gamma 3}$ and ΔE_U are relative to the global minimum of the conduction band, i.e. the bottom of the Γ_1 valley.

Symbol	Meaning	Value	Units
ϵ_0	Low freq. permittivity	8.9	
ϵ_∞	High freq. permittivity	5.35	
ω_{ph}	Opt. phonon energy	91	[meV]
D_{op}	Coupl. optical ph.	$3 \cdot 10^{11}$	[eV/m]
D_{ac}	Coupl. acoustic phonon	8.3	[eV]
$m_{\Gamma 1}$	Eff. mass. $\Gamma 1$ valley	0.2	[m_0]
$\alpha_{\Gamma 1}$	Non parab. $\Gamma 1$ valley	0.2	[eV^{-1}]
$m_{\Gamma 3}$	Eff. mass. $\Gamma 3$ valley	0.28	[m_0]
$\alpha_{\Gamma 3}$	Non parab. $\Gamma 3$ valley	0.2	[eV^{-1}]
$\Delta E_{\Gamma 3}$	Energy offset $\Gamma 3$ valley	2.2	[eV]
m_U	Eff. mass. U valleys	0.33	[m_0]
α_U	Non parab. U valleys	0.2	[eV^{-1}]
ΔE_U	Energy offset U valleys	2.0	[eV]

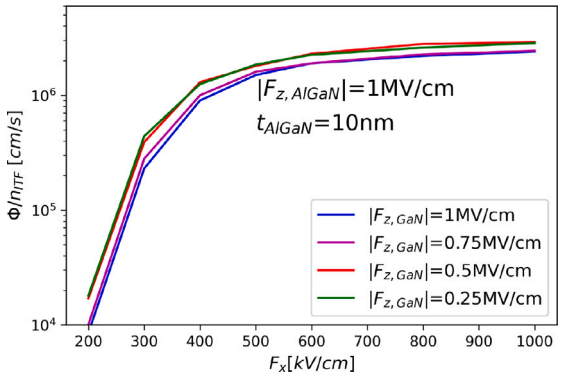

Fig. 2. Flux density of electrons into the passivation at the interface with AlGaN, Φ, normalized to the volumetric concentration in GaN at the interface with AlGaN, n_{ITF}, vs. the lateral electric field for different values of the vertical electric field in the GaN layer.

3. Results

Fig. 2 reports the electron flux density into the passivation at the interface with AlGaN, Φ, normalized to the volumetric electron density in the GaN at the interface with AlGaN, n_{ITF}, as a function of the lateral electric field. According to Gauss's Law F_x is the same in the GaN and AlGaN layers. Φ/n_{ITF} has units of a velocity and, remarkably, is independent of the vertical field in the GaN meaning that the injected flux is proportional to the volume density n_{ITF} at the interface, as in standard thermionic emission theory. When we change $F_{z,\mathrm{GaN}}$ we modify n_{ITF} (a larger field makes charges getting closer to the interface) but the injected flux changes by the same amount.

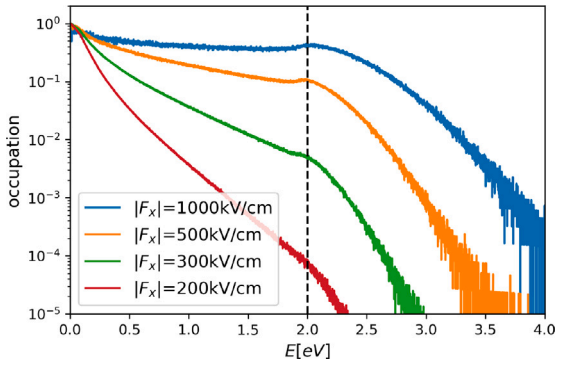

Fig. 3. Distribution function of electrons in the Γ_1 valley at the GaN/AlGaN interface. Dashed line: bottom of the U valleys. Distributions are normalized to be '1' at the bottom of the conduction band. The energy reference $E = 0$ eV is the bottom of the $\Gamma 1$ valley. As discussed in Section 2 Pauli's exclusion principle is not enforced and the actual distribution scales linearly with the assumed sheet density.

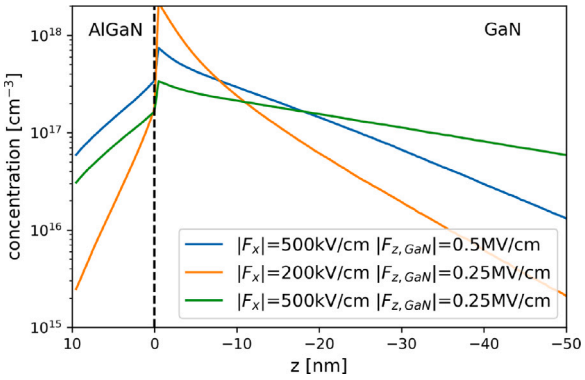

Fig. 4. Electron distribution along the vertical direction for different values of the electric field in AlGaN and GaN, for a 2DEG sheet concentration of $N_{2D} = 10^{12}$ cm^{-2}. $|F_{z,\mathrm{AlGaN}}| = 1$ MV/cm.

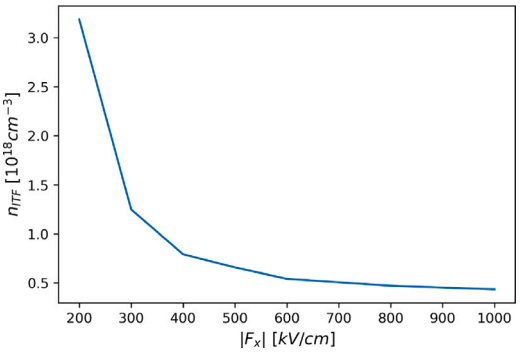

Fig. 5. Electron concentration at the GaN side of the AlGaN/GaN interface as a function of the lateral electric field, for a 2DEG sheet concentration of 10^{12} cm^{-2} (same as in Fig. 4). $F_{z,\mathrm{AlGaN}} = 1$ MV/cm. $F_{z,\mathrm{GaN}} = 0.5$ MV/cm.

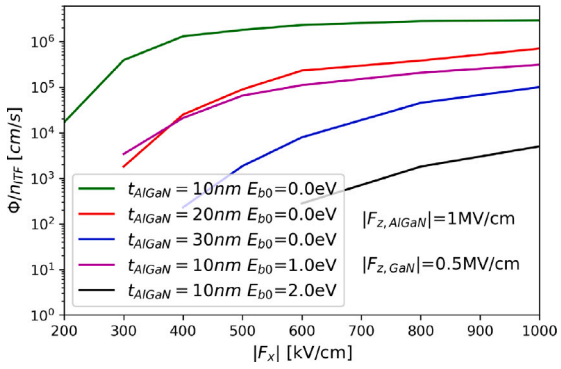

Fig. 6. Electron flux into the passivation Φ normalized to the concentration n_{ITF} in the GaN at the interface with AlGaN, for different AlGaN thicknesses and energy barriers at the passivation interface.

The flattening of the flux/concentration curves in Fig. 2 at large lateral field can be understood by examining Fig. 3, which shows $f(E)$ (the electron concentration per unit energy divided by the density of states) at the GaN side of the AlGaN/GaN interface. For $|F_x| > 500$ kV/cm, the occupation function is essentially flat below 2 eV, since below that energy, electrons are confined within the Γ_1 valley, where, due to the relatively low density of states, the energy loss rate is relatively low. Above this threshold, Γ_1-U intervalley scattering sets in, and electrons are transferred to the U valleys; due to the large availability of final states, net kinetic energy gain becomes more difficult, and the distribution function decreases rapidly for increasing energy. This explains why the curves in Fig. 2 (where the total barrier for injection in the passivation is 1.27 eV[1]) are essentially flat for lateral fields above ≈500 kV/cm. The inter-valley scattering between $\Gamma 1$ and the single $\Gamma 3$ valley, on the other hand, is much smaller than the one between $\Gamma 1$ and the six equivalent U valleys, and we have verified that the inclusion of the $\Gamma 3$ valley has a limited impact on the injected flux.

So far, we have shown in Fig. 2 the ratio between the electron flux density Φ injected into the passivation and the electron concentration n_{ITF} at the AlGaN/GaN interface. To assess the magnitude of the flux itself one needs to evaluate the electron concentration. A few concentration profiles along the vertical direction are shown in Fig. 4. The concentration is the highest at the AlGaN/GaN interface, and its decay in the vertical direction above and below the interface is a result of the balance between the vertical field in GaN and AlGaN, that oppose diffusion out of the potential well, and the lateral field that heats the electrons.

This latter aspect can be observed in Fig. 5, that plots the peak concentration as a function of the lateral electric field for given vertical fields. The values are below the effective density of states in the conduction band ($2.3 \cdot 10^{18}$cm^{-3}), that validates our choice to neglect degeneracy effect, i.e. to not enforce Pauli's exclusion principle. Note that in these simulations, $F_{z,\mathrm{GaN}}$ and $F_{z,\mathrm{AlGaN}}$ are treated as separate parameters, whereas in reality they are linked by the polarization charge.

Fig. 6 shows the ratio Φ/n_{ITF} for different AlGaN thicknesses and E_{b0}. The vertical electric field in the AlGaN is set to a typical value of 1 MV/cm, corresponding to a total barrier increase of 1 eV every 10 nm of t_{AlGaN}. We observe that increasing t_{AlGaN} from 10 nm to 20 nm and 30 nm, does not decrease the injected flux as much as increasing the barrier E_{b0} by steps of 1eV. This is because the electrons are heated by the lateral field in the AlGaN, and the kinetic energy initially gained along the x direction, is then redistributed in all directions by the isotropic and elastic alloy scattering. The effect is enhanced by increasing t_{AlGaN}. This point is analyzed with the help of Fig. 7: we see that the injection probability for given total energy barrier $(\Delta E_C + |F_{z,\mathrm{AlGaN}}| \cdot t_{\mathrm{AlGaN}})$ is much higher for large t_{AlGaN} compared to a case when the whole energy step is associated to ΔE_C.

[1] The sum of $\Delta E_C = 0.27$ eV and the product between t_{AlGaN} and $|F_{z,\mathrm{AlGaN}}|$. As we will see in at the end of this section, the effective barrier is even lower than that due to the effect of $|F_x|$.

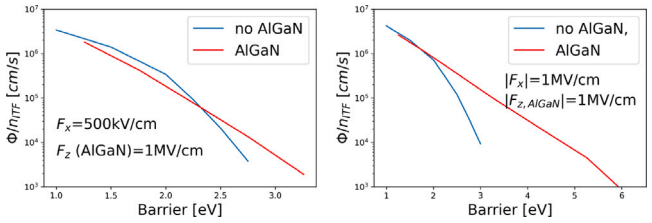

Fig. 7. Φ/n_{ITF} for $|F_x|$ = 500 kV/cm (left) and $|F_x|$ = 1000 kV/cm (rigth). The x-axis is the total energy barrier $\Delta E_C + |F_{z,\mathrm{AlGaN}}| t_{\mathrm{AlGaN}}$. In the blue curves no AlGaN layer is present and ΔE_C is varied as a parameters. In the red curves, instead, t_{AlGaN} is varied while keeping $|F_{z,\mathrm{AlGaN}}|$ = 1MV/cm to increase the total barrier (keeping ΔE_C = 0.27 eV).

4. Discussion and conclusions

The results in Fig. 6 suggest that engineering the passivation to increase E_{b0} is a more efficient way than increasing the AlGaN thickness to contain carrier injection in the passivation layer. However, for a full assessment of the trapping, one should consider the product between Φ/n_{ITF} (plotted in Figs. 2 and 6) and n_{ITF} itself. Considering as a relevant example E_{b0} = 2 eV, $\Phi/n_{ITF} \approx 10^3$ cm/s in Fig. 6 multiplied by a typical $n_{ITF} \approx 10^{17}\,\mathrm{cm}^{-3}$ (see Fig. 5), gives a flux of $\approx 10^{20}\,\mathrm{cm}^{-2}\,\mathrm{s}^{-1}$. This shows that the theoretically calculated injection rates are extremely high. However, the analysis proposed here provides the flux injected into the passivation: if the electric field therein is repulsive, most of the electrons will bounce back into the AlGaN, and only a fraction will get trapped. This implies that, to quantitatively predict the amount of charge trapped in the passivation, and the resulting dynamic-R_{on}, full-device simulations, as well as a model for the capture/release of hot electrons, in the passivation is needed. As future perspective, the model proposed here is currently being extended to perform full device simulations with realistic electric field profiles. Results will be presented in a future work accompanied by comparison with experimental dynamic R_{on} data.

CRediT authorship contribution statement

Pierpaolo Palestri: Writing – review & editing, Writing – original draft, Software, Methodology, Data curation, Conceptualization. **Luca Sayadi:** Writing – review & editing, Writing – original draft, Methodology, Conceptualization. **Andrea Minetto:** Writing – review & editing, Methodology, Conceptualization. **Gerhard Prechtl:** Writing – review & editing, Conceptualization. **Luca Selmi:** Writing – review & editing, Funding acquisition, Conceptualization. **Oliver Häberlen:** Writing – review & editing, Funding acquisition, Conceptualization.

Declaration of competing interest

The authors declare the following financial interests/personal relationships which may be considered as potential competing interests: Pierpaolo Palestri and Luca Selmi report financial support was provided by NextGeneration EU.The other authors declare that they have no known competing financial interests or personal relationships that could have appeared to influence the work reported in this paper.

Acknowledgments

This work received partial support by NextGeneration EU, Italian PNRR M4C2 1.5, ECOSISTER Spoke 3 Cascaded call E4PV project, CUP E93C22001100001.

Data availability

The data that has been used is confidential.

References

[1] Meneghini M, De Santi C, Abid I, Buffolo M, Cioni M, Khadar RA, Nela L, Zagni N, Chini A, Medjdoub F, Meneghesso G, Verzellesi G, Zanoni E, Matioli E. GaN-based power devices: Physics, reliability, and perspectives. J Appl Phys 2021;130(18):181101. http://dx.doi.org/10.1063/5.0061354.

[2] McDonald T. Power conversion semiconductor and circuit trends and challenges for a sustainable energy future. In: 2023 international electron devices meeting. IEDM, 2023, p. 1–4. http://dx.doi.org/10.1109/IEDM45741.2023.10413834.

[3] Yang S, Han S, Sheng K, Chen KJ. Dynamic on-resistance in GaN power devices: Mechanisms, characterizations, and modeling. IEEE J Emerg Sel Top Power Electron 2019;7(3):1425–39. http://dx.doi.org/10.1109/JESTPE.2019.2925117.

[4] Minetto A, Modolo N, Meneghini M, Zanoni E, Sayadi L, Sicre S, Deutschmann B, Häberlen O. Hot electron effects in AlGaN/GaN HEMTs during hard-switching events. Microelectron Reliab 2021;126:114208. http://dx.doi.org/10.1016/j.microrel.2021.114208, Proceedings of ESREF 2021, 32nd European Symposium on Reliability of Electron Devices, Failure Physics and Analysis.

[5] Zagni N, Verzellesi G, Bertacchini A, Borgarino M, Iucolano F, Chini A. Hole virtual gate model explaining surface-related dynamic RON in p-GaN power HEMTs. IEEE Electron Device Lett 2024;45(5):801–4. http://dx.doi.org/10.1109/LED.2024.3375912.

[6] Li K, Evans PL, Johnson CM. Characterisation and modeling of gallium nitride power semiconductor devices dynamic on-state resistance. IEEE Trans Power Electron 2018;33(6):5262–73. http://dx.doi.org/10.1109/TPEL.2017.2730260.

[7] Cioni M, Zagni N, Iucolano F, Moschetti M, Verzellesi G, Chini A. Partial recovery of dynamic RON versus OFF-state stress voltage in p-GaN gate AlGaN/GaN power HEMTs. IEEE Trans Electron Devices 2021;68(10):4862–8. http://dx.doi.org/10.1109/TED.2021.3105075.

[8] Moens P, Vanmeerbeek P, Banerjee A, Guo J, Liu C, Coppens P, Salih A, Tack M, Caesar M, Uren MJ, Kuball M, Meneghini M, Meneghesso G, Zanoni E. On the impact of carbon-doping on the dynamic ron and off-state leakage current of 650V GaN power devices. In: 2015 IEEE 27th international symposium on power semiconductor devices & iC's. ISPSD, 2015, p. 37–40. http://dx.doi.org/10.1109/ISPSD.2015.7123383.

[9] Uren MJ, Karboyan S, Chatterjee I, Pooth A, Moens P, Banerjee A, Kuball M. "Leaky Dielectric" model for the suppression of dynamic R_{ON} in carbon-doped AlGaN/GaN HEMTs. IEEE Trans Electron Devices 2017;64(7):2826–34. http://dx.doi.org/10.1109/TED.2017.2706090.

[10] Joshi V, Roy Chaudhuri R, Dutta Gupta S, Shrivastava M. Physical insights into electron trapping mechanism in the carbon-doped GaN buffer in AlGaN/GaN HEMTs and its impact on dynamic on-resistance. IEEE Trans Electron Devices 2023;70(6):3011–8. http://dx.doi.org/10.1109/TED.2023.3269409.

[11] Yang F, Dalcanale S, Gajda M, Karboyan S, Uren MJ, Kuball M. The impact of hot electrons and self-heating during hard-switching in AlGaN/GaN HEMTs. IEEE Trans Electron Devices 2020;67(3):869–74. http://dx.doi.org/10.1109/TED.2020.2968212.

[12] Favero D, De Santi C, Stockman A, Nardo A, Vanmeerbeek P, Tack M, Meneghesso G, Zanoni E, Meneghini M. R_{ON} and V_{TH} extraction in hard-switched E-mode GaN HEMTs: Impact of passivation and layout. In: 2024 IEEE international reliability physics symposium. IRPS, 2024, p. 1–4. http://dx.doi.org/10.1109/IRPS48228.2024.10529377.

[13] Minetto A, Modolo N, Meneghini M, Zanoni E, Sayadi L, Sicre S, Deutschmann B, Häberlen O. Hot electron effects in AlGaN/GaN HEMTs during hard-switching events. Microelectron Reliab 2021;126:114208.

[14] Nakajima A, Yagi S, Shimizu M, Adachi K, Okumura H. Hot electron induced current collapse in algan/gan HEMTs. In: Materials science forum. vol. 556, Trans Tech Publ; 2007, p. 1035–8.

[15] Albrecht JD, Wang RP, Ruden PP, Farahmand M, Brennan KF. Electron transport characteristics of GaN for high temperature device modeling. J Appl Phys 1998;83(9):4777–81. http://dx.doi.org/10.1063/1.367269.

[16] Bhapkar UV, Shur MS. Monte Carlo calculation of velocity-field characteristics of wurtzite GaN. J Appl Phys 1997;82(4):1649–55. http://dx.doi.org/10.1063/1.365963.

[17] Vitanov S, Nedjalkov M, Palankovski V. A Monte Carlo model of piezoelectric scattering in GaN. In: Boyanov T, Dimova S, Georgiev K, Nikolov G, editors. Numerical methods and applications. Berlin, Heidelberg: Springer Berlin Heidelberg; 2007, p. 197–204.

[18] Wang S, Wu Z, Haifeng Z, Duan X, Han C, Wei Y, Liu H. Comparison the electron momentum and energy relaxation process in wurtzite gan, InN and AlN by Monte Carlo method. Solid State Commun 2019;288:68–73. http://dx.doi.org/10.1016/j.ssc.2018.11.018.

[19] Fang J, Fischetti MV, Schrimpf RD, Reed RA, Bellotti E, Pantelides ST. Electron transport properties of $Al_xGa_{1-x}N$/GaN transistors based on first-principles calculations and Boltzmann-equation Monte Carlo simulations. Phys Rev Appl 2019;11:044045. http://dx.doi.org/10.1103/PhysRevApplied.11.044045.

[20] Miyazaki W, Tanaka H, Mori N. Full-band Monte Carlo analysis of strain effects on carrier transport in GaN. Japan J Appl Phys 2024;63(2):02SP35. http://dx.doi.org/10.35848/1347-4065/ad1005.

[21] Bertazzi F, Moresco M, Bellotti E. Theory of high field carrier transport and impact ionization in wurtzite gan. Part I: A full band Monte Carlo model. J Appl Phys 2009;106(6):063718. http://dx.doi.org/10.1063/1.3213363.